



HAL
open science

Generation and backreaction of spontaneously emitted inertia-gravity waves

Norihiko Sugimoto, Riwal Plougonven

► **To cite this version:**

Norihiko Sugimoto, Riwal Plougonven. Generation and backreaction of spontaneously emitted inertia-gravity waves. *Geophysical Research Letters*, 2016, 43, pp.3519-3525. 10.1002/2016GL068219 . insu-03727114

HAL Id: insu-03727114

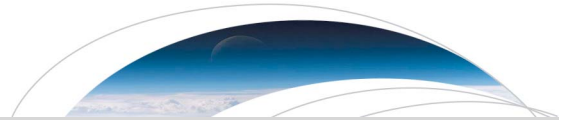
<https://hal-insu.archives-ouvertes.fr/insu-03727114>

Submitted on 19 Jul 2022

HAL is a multi-disciplinary open access archive for the deposit and dissemination of scientific research documents, whether they are published or not. The documents may come from teaching and research institutions in France or abroad, or from public or private research centers.

L'archive ouverte pluridisciplinaire **HAL**, est destinée au dépôt et à la diffusion de documents scientifiques de niveau recherche, publiés ou non, émanant des établissements d'enseignement et de recherche français ou étrangers, des laboratoires publics ou privés.

Copyright



RESEARCH LETTER

10.1002/2016GL068219

Key Points:

- Maximum wave vertical velocity is proportional to the resolution
- The energy extracted by the waves is weakly sensitive to the resolution
- The dipole loses at most 0.2% energy per day to inertia-gravity waves

Supporting Information:

- Supporting Information S1

Correspondence to:

N. Sugimoto,
nori@phys-h.keio.ac.jp

Citation:

Sugimoto, N., and R. Plougonven (2016), Generation and backreaction of spontaneously emitted inertia-gravity waves, *Geophys. Res. Lett.*, *43*, 3519–3525, doi:10.1002/2016GL068219.

Received 10 FEB 2016

Accepted 20 MAR 2016

Accepted article online 24 MAR 2016

Published online 6 APR 2016

Generation and backreaction of spontaneously emitted inertia-gravity waves

Norihiko Sugimoto¹ and Riwal Plougonven²

¹Research and Education Center for Natural Sciences, Department of Physics, Keio University, Yokohama, Japan,

²Laboratoire de Météorologie Dynamique, École polytechnique, Université Paris Saclay, Palaiseau, France

Abstract Spontaneous generation of inertia-gravity waves from balanced flows is investigated in idealized simulations of dipoles. Long integrations are performed for dipoles with different Rossby numbers (Ro) to identify the backreaction of the waves. Emission of waves is detected only for large enough Ro (>0.15), and it then leads to a slow decay of the dipole's kinetic energy. A major finding is that this decay is well captured by the simulations, although positions of the waves appear still sensitive to the resolution, and their maximum vertical velocity increases linearly with resolution. The interpretation is that the emission process is well resolved and fairly insensitive to resolution, while the propagation and dissipation at small scales remains sensitive to resolution. The implication is that the simulations yield an estimate of the leakage of energy from balanced motions to gravity waves, providing a useful estimate of a poorly constrained flux in the ocean's energy budget.

1. Introduction

Inertia-gravity waves (IGWs) play important roles in both the atmosphere and ocean, through their momentum fluxes and the resulting forcing of the middle atmosphere's circulation [Fritts and Alexander, 2003], and as a pathway for energy toward small scales where dissipation can occur in the ocean [Ferrari and Wunsch, 2009]. Their small scales are such that they need to be parameterized [Kim *et al.*, 2003; Polzin *et al.*, 2014], requiring a good fundamental understanding of their dynamics, from their sources to their dissipation. A persistent difficulty has concerned nonorographic waves generated by the dynamics near jets and fronts [see Plougonven and Zhang, 2014], which is tied to the difficult and fundamental issue of gravity wave generation from balanced motions, or "spontaneous generation," see Vanneste [2013] for a review.

Consistent with many observations [e.g., Uccellini and Koch, 1987; Guest *et al.*, 2000], idealized simulations have confirmed jet exit regions as a key location for gravity wave generation in baroclinically unstable systems [e.g., O'Sullivan and Dunkerton, 1995; Zhang, 2004; Zülicke and Peters, 2006; Plougonven and Snyder, 2007]. The generation of such waves has been understood in idealized simulations of dipoles [Snyder *et al.*, 2007; Viúdez, 2007; Wang *et al.*, 2009; Yasuda *et al.*, 2015b] as the linear response on the background of the dipole flow to the small deviations from balance that are inevitably present at finite Rossby number (Ro) [Snyder *et al.*, 2009; Wang and Zhang, 2010; Yasuda *et al.*, 2015a]. Propagation effects, due to the exit region's deformation and shear, have been shown to strongly influence the intrinsic frequency and orientation of the waves [Bühler and McIntyre, 2005; Plougonven and Snyder, 2005; Wang *et al.*, 2009], but the wave-mean flow implications of this "wave capture" remain uncertain [McIntyre, 2009]. Uncertainties also remain regarding the amplitudes of the emitted waves, with idealized simulations still sensitive to the resolution and showing a discrepancy with respect to observed amplitudes [e.g., Pavelin *et al.*, 2001; Plougonven *et al.*, 2003; Zülicke and Peters, 2008].

The present study revisits the emission of gravity waves in a dipole, using long-term simulation to identify the backreaction of the waves on the dipole. The use of a more accurate balanced initial state and of a spectral model with small horizontal hyperdiffusion make it possible to conduct numerical simulations on longer times (section 2). The continuous, weak emission of IGWs which are squeezed in the jet exit to the smallest available scales leads to enhanced dissipation for finite Ro (section 3). The dependence on Ro and on resolution allows to estimate an upper bound for the rate at which spontaneous emission leaks energy from the dipole. The implications for the ocean's energy budget are discussed, providing a revised figure for the energy flux due to spontaneous imbalance from balanced mesoscale eddies (section 4).

2. Experimental Setup

The numerical model used is DCPAM5 plane (Dennou-Club Planetary Atmospheric Model [Takehiro *et al.*, 2011]) which solves the dry primitive equations on an f plane with a sigma coordinate in the vertical. The

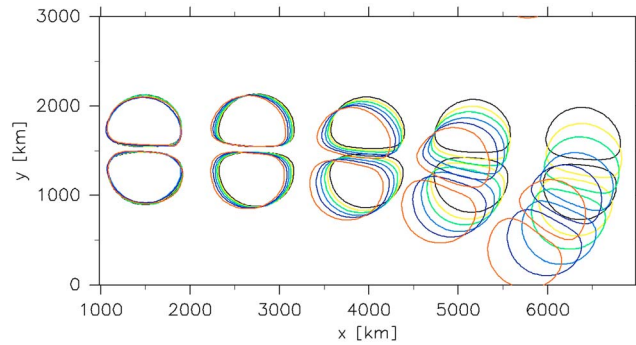


Figure 1. The positions of the dipoles at day 0, $7 \times (0.3/Ro)$, $14 \times (0.3/Ro)$, $21 \times (0.3/Ro)$, and $28 \times (0.3/Ro)$ for different Ro cases. Each color contour line expresses surface pressure disturbances with $\pm 60 \times (Ro/0.3)$ Pa, indicating the positions of the cyclone and anticyclone for each dipole. Each color shows different Ro cases; $Ro = 0.05$ (black), 0.1 (yellow), 0.15 (green), 0.2 (light blue), 0.25 (blue), and 0.3 (red).

domain is 3000 km times 3000 km in horizontal and 20 km in the vertical direction. The control run has 128^2 grid points and 80 layers, which corresponds to a resolution of ~ 23.4 km in the horizontal and ~ 250 m in the vertical. The boundary conditions are doubly periodic in the horizontal and rigid in upper and lower boundaries. A sponge layer is included above 15 km, and we have verified with sensitivity experiments that it leaves the dipole unaffected.

The initial condition is an exact dipole solution derived analytically in the quasi-geostrophic approximation [Muraki and Snyder, 2007]. This dipole moves steadily eastward and is trapped on the surface.

As an extension of the previous study [Snyder et al., 2007], the following ageostrophic winds deduced from geostrophic advection are added:

$$\mathbf{u}_a = (u_a, v_a) = (-f^{-1} \mathbf{u}_g \nabla v_g, -f^{-1} \mathbf{u}_g \nabla u_g), \quad (1)$$

where $\mathbf{u}_g = (u_g, v_g)$ is the geostrophic velocity. These additional terms make the dipole trajectories straighter than those described in Snyder et al. [2007]. The horizontal length scale of the dipole, i.e., its radius $L = 500$ km, is fixed. The values of the background environment are also fixed ($f = 10^{-4} \text{ s}^{-1}$ for the Coriolis parameter, $N = 10^{-2} \text{ s}^{-1}$ for the Brunt-Väisälä frequency, and $\theta_0/g = 30.6 \text{ K m}^{-1} \text{ s}^2$ for the ratio of the reference potential temperature to the gravitational acceleration).

To quantify the generation of IGWs at various Rossby numbers, numerical simulations with six different strengths of the dipoles ($U_0 = 2.5, 5.0, 7.5, 10.0, 12.5,$ and 15.0 m s^{-1} , where U_0 is the maximum wind) are performed. The corresponding Rossby numbers, $Ro \equiv U_0/fL$, are 0.05, 0.1, 0.15, 0.2, 0.25, and 0.3, respectively. The phase speeds are $\sim 2.07 \times (Ro/0.3) \text{ m s}^{-1}$. In order to detect a possible backreaction of IGWs toward the dipole, long time integrations are required to find a cumulative effect of the waves. For this purpose, time integration is performed for 84 days with $Ro = 0.30$ using a time step $\Delta t = 300$ s. For the other simulations, the duration time is extended ($84 \times (0.3/Ro)$ days) to compensate for the dipole's weakness: e.g., the simulation with $Ro = 0.15$ lasts twice as long (168 days). The model includes fourth-order horizontal hyperdiffusion which only acts on small scales. The e -folding time of the horizontal hyperdiffusion also depends on Ro , namely, $0.1 \times (0.3/Ro)$ days. With this setup, if the dipoles were purely quasi-geostrophic, their trajectories would be the same. Differences that arise between the different runs come from higher-order corrections to quasi-geostrophy and from spontaneously generated IGWs.

In order to thoroughly test the sensitivity of the dipole's behavior to resolution and to hyperdiffusion, many other numerical simulations with different resolutions ($64^2, 96^2, 192^2,$ and 256^2 horizontal grids with 80 vertical layers and 128^2 horizontal grids with 160 vertical layers) were performed for the case of $Ro = 0.3$.

3. Results

The time series of the positions of the dipoles (for the first third of the trajectories) for different Ro cases are shown in Figure 1. As Ro increases, the dipoles veer more anticyclonically. As robust, stable structures that propagate quasi-steadily, the dipoles provide a unique opportunity to quantify the generation and backreaction of IGWs at jet exit region.

Clear generation of IGWs at the jet exit region is observed only for large enough Ro (>0.15). Figures 2a–2c show an example of IGWs for $Ro = 0.15$ at day 42. Total vertical velocity w is decomposed into large-scale (k and $l \leq 6$) and small-scale (k or $l \geq 11$) components by spatial filtering in a horizontal Fourier space to quantify IGWs, where k and l are the horizontal wave numbers. While the large-scale vertical velocity is mainly part

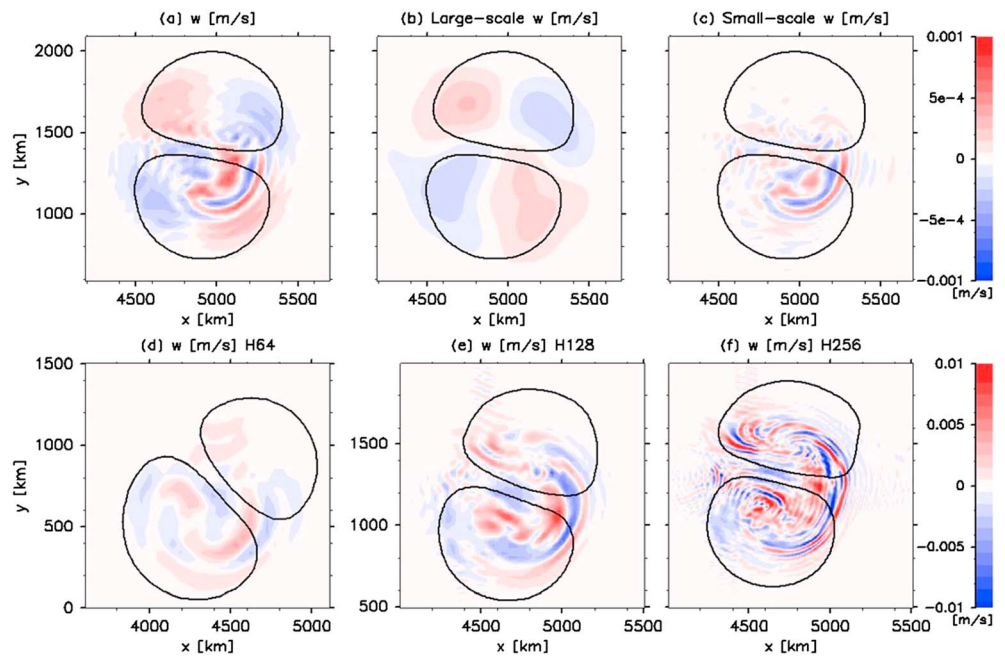


Figure 2. Horizontal sections at $z = 125$ m of (a) vertical velocity w (color shades, m s^{-1}), (b) its large-scale component, and (c) small-scale component for $Ro = 0.15$ at day 42. The dependence of w on the horizontal resolution: (d) lower resolution (64^2 horizontal grids), (e) control (128^2 horizontal grids), and (f) higher resolution (256^2 horizontal grids) runs for $Ro = 0.3$ at day 21. Black contour lines indicate the positions of the cyclone and anticyclone for each dipole by surface pressure disturbances with ± 30 Pa (Figures 2a–2c) and ± 60 Pa (Figures 2d–2f).

of the balanced flow, the small-scale vertical velocity is the signature of the IGWs generated in the jet and then advected and propagating downstream. A packet of IGW is present in the front of the dipole, and it extends into the anticyclone. The overall structure of IGWs, such as positions and cyclone-anticyclone asymmetry, is consistent with previous studies with different numerical models and experimental settings [e.g., Snyder et al., 2007; Viúdez, 2007; Wang et al., 2009; Yasuda et al., 2015a].

The dependence of IGWs on the resolution is also illustrated in Figures 2d–2f. The run with higher resolution resolves small-scale IGWs more and more, and amplitudes of IGWs increase also (Figure 2f). Nevertheless, the fundamental structure of the IGWs, namely, the main wave packet in the jet exit region and wrapping strongly in the anticyclone, is the same as in the control run (Figure 2d).

The wave characteristics show significant sensitivity: the wavelengths are mainly sensitive to the resolution, and the amplitudes are sensitive to both Ro and the resolution. In the control runs for $Ro = 0.15$ and 0.3 ($U_0 = 7.5$ and 15.0 m s^{-1} , respectively), the maximum values of small-scale horizontal wind disturbances are $|\mathbf{u}'| \sim 0.1$ and $\sim 0.5 \text{ m s}^{-1}$, respectively, while the typical wavelengths in the jet exit region are similar: $\lambda_h \sim 70 \text{ km}$ in the horizontal and $\lambda_z \sim 0.5 \text{ km}$ in the vertical. Those values agree with the previous numerical simulations [e.g., Snyder et al., 2007], although the model used is completely different. At higher resolution (256^2 horizontal grid points) for $Ro = 0.3$, amplitudes of IGWs increase to $|\mathbf{u}'| \sim 1.0 \text{ m s}^{-1}$ and the horizontal wavelength decreases to $\lambda_h \sim 35 \text{ km}$, while the vertical wavelength $\lambda_z \sim 0.5 \text{ km}$ remains similar.

The dependence of the amplitudes of IGWs on the Ro , quantified by the maximum absolute values of the vertical velocity (w_{max}) at day $21 \times (0.3/Ro)$, is plotted in Figure 3a. First, it is clearly seen that IGWs are detectable only for $Ro > 0.15$. The amplitudes of IGWs follow a law of Ro to the power of 3.5, while the large-scale balanced w varies as the square of Ro , which is consistent with previous studies [Snyder et al., 2007; Yasuda et al., 2015b].

The resolution dependence of w_{max} and of the large- and small-scale components of the vertical velocity is plotted in Figure 3b. The balanced (large-scale) component shows only a weak sensitivity to resolution (this likely differs in more complex flows such as baroclinic life cycles, which includes frontogenesis [e.g., Mirzaei et al., 2014]). Remarkably, the maximum vertical velocity of the waves has a linear dependence on the

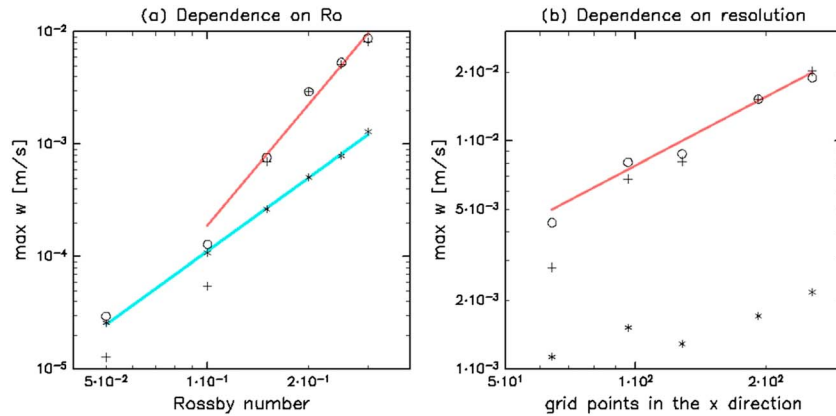


Figure 3. Dependences on the (a) Ro and (b) resolution of the maximum absolute values of the vertical velocity w (denoted by circle), their large-scale components (denoted by asterisk), and their small-scale components (denoted by plus sign) at $z = 125$ m at day $21 \times (0.3/Ro)$. Lines in Figure 3a with slope of 3.49 (red) and 2.17 (blue light) are best fit by the least squares method. Line in Figure 3b with slope of 2 (red) is proportional to the resolution.

resolution. This can be understood qualitatively as follows: we assume that the energy of IGW packet, E_{IGW} , is insensitive to the resolution. The waves' energy may be written as follows:

$$E_{IGW} = \frac{\rho}{2} (\hat{u}^2 + \hat{w}^2) + N^2 \hat{\theta}^2 = \frac{\rho}{2} \hat{w}^2 \left(\frac{m^2}{k^2} + 1 \right) + N^2 \hat{\theta}^2 \sim \frac{\rho}{2} \hat{w}^2 \left(\frac{m^2}{k^2} \right), \quad (2)$$

where ρ is the density, \hat{u} and \hat{w} indicate the amplitude of horizontal and vertical velocity fluctuations induced by IGW, and k and m are the horizontal and vertical wave numbers of IGW. As shown in Figures 2d–2f, when the horizontal resolution is doubled, the horizontal wavelength becomes half ($k \rightarrow 2k$), while the vertical wavelength is quite insensitive. Hence, in order to keep the energy unchanged in the expression above, one needs the vertical velocity to be doubled ($\hat{w} \rightarrow 2\hat{w}$). The implication of the above argument is that the sensitivity of the maximum vertical velocity to resolution behaves as expected and is perhaps not an obstacle to conclusive statements on the intensity of spontaneous emission for the present simulations. Sensitivity to the vertical resolution has also been tested and is much weaker than sensitivity to the horizontal resolution.

We now turn to the long-term evolution of the dipole and to the backreaction of the waves. For $Ro = 0.3$ the dipole progressively veers southward; it almost goes to the south at day 46 and to the west at day 74. Figures 4a and 4b show that their structures rotated by 90 and 180°, respectively. While amplitudes of IGWs very slightly decrease, the overall structure at day 74 is remarkably similar to that at day 46. This continuous emission of gravity waves causes slow decay of the dipole.

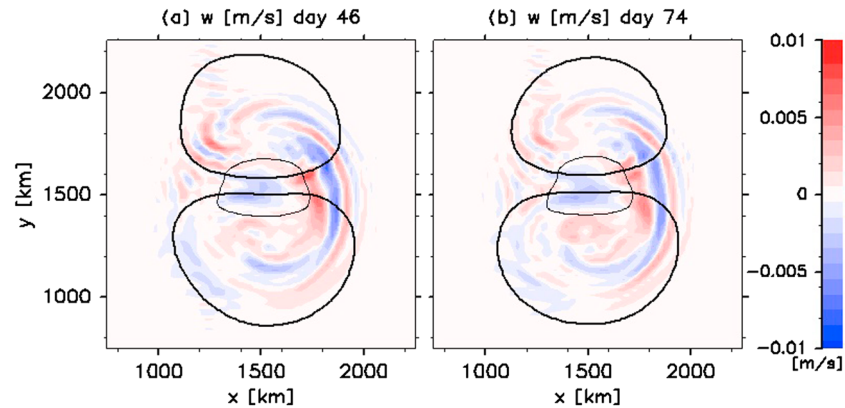


Figure 4. Snapshots of the dipole for $Ro = 0.3$ in the long-term evolution. Vertical velocity (color shades, $m s^{-1}$) at $z = 125$ m at (a) day 46 and (b) day 74. Dipoles are moved to the center of the domain and rotated by 90° for Figure 4a and 180° for Figure 4b. Black contour lines indicate the positions of the cyclone and anticyclone for each dipole by surface pressure disturbances with ± 60 Pa. The surface isotach corresponding to $|u| = 10 m s^{-1}$ are also shown by thin contour lines.

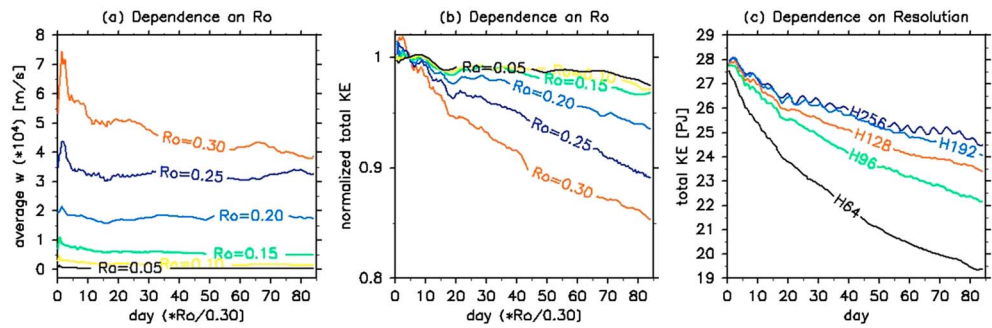


Figure 5. Time evolutions of (a) the root-mean-square of the vertical velocity w (m s^{-1}), (b) total horizontal kinetic energy (TKE) of the dipoles for the cases from $Ro = 0.05$ to 0.3 , and (c) TKE ($\text{PJ} = 10^{15} \text{ J}$) for $Ro = 0.3$ cases with different resolution. In Figures 5a and 5b, each color represents different Ro cases; $Ro = 0.05$ (black), 0.1 (yellow), 0.15 (green), 0.2 (light blue), 0.25 (blue), and 0.3 (red). In Figure 5c, each color represents different resolution cases; 64^2 (black), 96^2 (green), 128^2 (red), 192^2 (light blue), and 256^2 (blue) horizontal grid points. In Figures 5a and 5b, day is normalized by Ro . In Figure 5b, TKE is also normalized by initial 5 days mean.

The backreaction of the waves on the dipole come out in the time series of the root-mean-square of the vertical velocity ($\langle w \rangle$) and of the total horizontal kinetic energy $\text{TKE} = \int V \frac{\rho(u^2+v^2)}{2} dV$, which are shown for different Ro cases in Figures 5a and 5b, respectively. For the cases from $Ro = 0.05$ to 0.25 , $\langle w \rangle$ almost remains unchanged, except for large fluctuations in an early period, caused by the initial geostrophic adjustment. For $Ro = 0.30$, $\langle w \rangle$ gradually decreases, but still it is larger than that for $Ro = 0.25$ even at the end of the simulation. In contrast, TKE decreases significantly for large Ro (> 0.15) where the generation of IGWs observed, whereas TKE is almost conserved (more than 96%) for small Ro (≤ 0.15). The individual setting of the hyperdiffusion with different Ro guarantees that this is not attributed to the dissipation only. Therefore, this decay of the dipole's energy is caused by the continuous radiation of IGWs, and it allows to quantify this emission.

Now the dependence of TKE on the resolution is shown in Figure 5c for $Ro = 0.30$ cases. Remarkably, the results of the runs with higher resolution (192^2 and 256^2 horizontal grids) almost converge, which suggest that the flux of energy extracted by the emitted IGWs is well resolved. This is consistent with the understanding of the emission process [Snyder et al., 2009; McIntyre, 2009] which is driven by large-scale fields (both for the forcing and advection). In contrast, the subsequent propagation of the waves, their contraction at the front of the jet exit region, and ultimate dissipation at the smallest available scales depend on the resolution, as would the smallest scales of a passive scalar [Bühler and McIntyre, 2005]. Whether fitting linearly or fitting to an exponential decay, we find a flux of energy removed from the balanced flow of the order of $0.2\% \text{ d}^{-1}$.

Finally, we have investigated the sensitivity to the horizontal hyperdiffusion. While the trajectories of the dipoles remain almost indistinguishable, $\langle w \rangle$ increases in runs with hyperdiffusion weaker than in the control run. However, the spectral analysis reveals that this corresponds to a spurious accumulation of energy at the finest resolvable scale (Figure S1 in the supporting information). Our values for the hyperdiffusion were chosen as a compromise to avoid this and to leave the dipole unaffected.

4. Summary and Discussion

The present study revisits the spontaneous generation of inertia-gravity waves (IGWs) in a jet exit region using idealized simulations of dipoles to confirm the robustness of the phenomenology previously described for the emission (present for $Ro > 0.15$, maximum vertical velocity proportional to the 3.5th power of Ro).

Going beyond previous investigations, we have explored the long-term behavior of the emitted wave packet and of the dipole and extensively tested the sensitivity of the simulations to resolution and dissipation. The wave packet is confirmed as a very stable component of the dipole, quasi-stationary in time with respect to the moving dipole. Deviation from stationarity comes from the slow decay of the dipole, which results from emission of the waves. For $Ro < 0.15$, the dipole is found not to weaken despite very long integration times. For $Ro > 0.15$, the energy of the dipole decays with time, this decay increasing with Ro .

Previous investigations have been plagued by a sensitivity to resolution that has prevented robust conclusions regarding the amplitudes of spontaneously emitted waves [O'Sullivan and Dunkerton, 1995; Plougonven and Snyder, 2005, 2007; Snyder et al., 2007]. Our main findings are as follows: the waves indeed appear quite sensitive to resolution, with increased resolution leading to larger maximum vertical velocity at the front of the dipole. In contrast, the long-term behavior of the dipole has only a weak sensitivity to resolution: the decay of the dipole's kinetic energy converges at high resolution. Both lines of results support the following interpretation: the emission of the waves is well resolved for resolutions 192^2 or larger. This results from the large-scale character of the fields involved in the generation [e.g., Snyder et al., 2009; see also O'Sullivan and Dunkerton, 1995]. Once emitted, the waves propagate in a strong strain which produces fine horizontal wavelengths, those being very sensitive to resolution. Simple considerations on the energy of the wave packet show that with the energy of the incoming wave packet unchanged (i.e., with emission well resolved), the maximum vertical velocity in the front of the wave packet will increase linearly with the resolution (see Figure 3 and equation (2)). This agrees remarkably with the numerical results.

In summary, the above explains the sensitivity of the wave's signature in vertical velocity and also provides evidence for a robust estimation of the energy extracted from the dipole by the waves. This estimation is useful for the debate on the energy budget of the ocean's interior, and we now turn to this topic.

Over the past two decades an important debate in oceanography bears on the energy budget of the ocean's circulation [Ferrari and Wunsch, 2009, and references therein]. Input of energy from the wind forcing at the surface has to be compensated by sinks of energy, but quantifying them remains very uncertain. A major reservoir of kinetic energy is made of the balanced eddies in the ocean's interior (total energy is estimated at about 13×10^{18} J or 13 EJ), and much uncertainty remains on pathways for energy down to small scales where it can be dissipated. Laboratory experiments [Williams et al., 2008] displaying spontaneous generation have been used to extrapolate a possible flux of energy from balanced motions to gravity waves, as a first step for a cascade down to small scales, yielding a value of up to 1.5 TW. Although this estimate has limitations, it regularly serves as a reference point in the debate [Ferrari and Wunsch, 2010, Brüggemann and Eden, 2015] for lack of other estimates. Our simulations have the advantage of describing a continuously stratified flow and reproducing a phenomenology highlighted as a paradigm for spontaneous generation from both observations and idealized simulations [Plougonven and Zhang, 2014]. We estimate a maximal flux of energy from the balanced motions of $0.2\% \text{ d}^{-1}$. Applied to the interior, geostrophic eddy field, this yields a flux of energy of about 0.3 TW. Three limitations need to be emphasized: first, more complex flows may generate stronger gravity waves, although there is fragmentary evidence that such increase would not be very large [Afanasyev, 2003; Danioux et al., 2012]. Second, the estimate above is based on the emission found for strong dipoles (decaying jets), with $Ro = 0.3$, for fixed diffusion and stratification. For Ro weaker than 0.15, emitted waves could not be detected, and it is presumably even weaker $Ro (< 0.1)$ and monopoles (decaying eddies) that are relevant for the ocean's interior. Third, kinetic energy in the balanced eddies would be only several tens of percent of the total energy. We therefore suggest that the estimate of the flux of energy due to spontaneous emission should be revised to a value weaker than the 1 TW often considered. In agreement with Brüggemann and Eden, [2015], a value of 0.3 TW seems more plausible, and it is likely an upper bound still.

Acknowledgments

The data from the simulations are available upon request from the corresponding author. The work by N.S. is supported by the Grant-in-Aid for Young Scientists (B) (25800265) and Scientific Research (A) (25247075) of the Ministry of Education, Culture, Sports and Technology (MEXT), Japan. R.P. acknowledges support from the StraDyVariUS project (ANR-13-BS06-0011-01) funded by ANR. N.S. thanks S. Takehiro, Y. Yasuda, and K. Sato, and R.P. is grateful to C. Snyder, for stimulating discussions in early stages of this work. We thank two anonymous referees for their constructive comments and are grateful to Laboratoire de Météorologie Dynamique for hosting N.S. The GFD-DENNOU Library was used for creating figures.

References

- Afanasyev, Y. (2003), Spontaneous emission of gravity waves by interacting vortex dipoles in a stratified fluid: Laboratory experiments, *Geophys. Astrophys. Fluid Dyn.*, *97*, 79–95.
- Brüggemann, N., and C. Eden (2015), Routes to dissipation under different dynamical conditions, *J. Phys. Oceanogr.*, *45*, 2149–2168.
- Bühler, O., and M. E. McIntyre (2005), Wave capture and wave-vortex duality, *J. Fluid Mech.*, *534*, 67–95.
- Danioux, E., J. Vanneste, P. Klein, and H. Sasaki (2012), Spontaneous inertia-gravity wave generation by surface-intensified turbulence, *J. Fluid Mech.*, *699*, 153–173.
- Ferrari, R., and C. Wunsch (2009), Ocean circulation kinetic energy: Reservoirs, sources and sinks, *Annu. Rev. Fluid Mech.*, *41*, 253–82.
- Ferrari, R., and C. Wunsch (2010), The distribution of eddy kinetic and potential energies in the global ocean, *Tellus*, *62A*, 92–108.
- Fritts, D. C., and M. J. Alexander (2003), Gravity wave dynamics and effects in the middle atmosphere, *Rev. Geophys.*, *41*(1), 1003, doi:10.1029/2001RG000106.
- Guest, F., M. J. Reeder, C. Marks, and D. Karoly (2000), Inertia-gravity waves observed in the lower stratosphere over Macquarie Island, *J. Atmos. Sci.*, *57*, 737–752.
- Kim, Y.-J., S. Eckermann, and H.-Y. Chun (2003), An overview of the past, present and future of gravity-wave drag parametrization for numerical climate and weather prediction models, *Atmos. Ocean*, *41*, 65–98.
- McIntyre, M. E. (2009), Spontaneous imbalance and hybrid vortex-gravity structures, *J. Atmos. Sci.*, *66*, 1315–1325.

- Mirzaei, M., C. Zülicke, A. R. Mohebalhojeh, F. Ahmadi-Givi, and R. Plougonven (2014), Structure, energy and parameterization of inertia-gravity waves in dry and moist simulations of a baroclinic wave life cycle, *J. Atmos. Sci.*, *71*, 2390–2414.
- Muraki, D. J., and C. Snyder (2007), Vortex dipoles for surface quasigeostrophic models, *J. Atmos. Sci.*, *64*, 2961–2967.
- O'Sullivan, D., and T. J. Dunkerton (1995), Generation of inertia-gravity waves in a simulated life cycle of baroclinic instability, *J. Atmos. Sci.*, *52*, 3695–3716.
- Pavelin, E., J. A. Whiteway, and G. Vaughan (2001), Observation of gravity wave generation and breaking in the lowermost stratosphere, *J. Geophys. Res.*, *106*, 5173–5179, doi:10.1029/2000JD900480.
- Plougonven, R., and C. Snyder (2005), Gravity waves excited by jets: Propagation versus generation, *Geophys. Res. Lett.*, *32*, L18802, doi:10.1029/2005GL023730.
- Plougonven, R., and C. Snyder (2007), Inertia-gravity waves spontaneously generated by jets and fronts. Part I: Different baroclinic life cycles, *J. Atmos. Sci.*, *64*, 2502–2520.
- Plougonven, R., and F. Zhang (2014), Internal gravity waves from atmospheric jets and fronts, *Rev. Geophys.*, *52*, 33–76, doi:10.1002/2012RG000419.
- Plougonven, R., H. Teitelbaum, and V. Zeitlin (2003), Inertia-gravity wave generation by the tropospheric midlatitude jet as given by the FASTEX radiosoundings, *J. Geophys. Res.*, *108*(D21), 4686, doi:10.1029/2003JD003535.
- Polzin, K. L., A. C. N. Garabato, T. N. Huussen, B. M. Sloyan, and S. Waterman (2014), Finescale parameterizations of turbulent dissipation, *J. Geophys. Res. Oceans*, *119*, 1383–1419, doi:10.1002/2013JC008979.
- Snyder, C., D. J. Muraki, R. Plougonven, and F. Zhang (2007), Inertia-gravity waves generated within a dipole vortex, *J. Atmos. Sci.*, *64*, 4417–4431.
- Snyder, C., R. Plougonven, and D. J. Muraki (2009), Forced linear inertia-gravity waves on a basic-state dipole vortex, *J. Atmos. Sci.*, *66*, 3464–3478.
- Takehiro, S., Y. O. Takahashi, M. Odaka, M. Ishiwatari, K. Nakajima, Y.-Y. Hayashi, and dcpam5-plane development Group (2011), dcpam5-plane: A planetary atmosphere model, GFD Dennou Club. [Available at <http://www.gfd-dennou.org/library/dcpam/>]
- Uccellini, L. W., and S. E. Koch (1987), The synoptic setting and possible energy sources for mesoscale wave disturbances, *Mon. Weather Rev.*, *115*, 721–729.
- Vanneste, J. (2013), Balance and spontaneous wave generation in geophysical flows, *Annu. Rev. Fluid Mech.*, *45*, 147–172.
- Viúdez, Á. (2007), The origin of the stationary frontal wave packet spontaneously generated in rotating stratified vortex dipoles, *J. Fluid Mech.*, *593*, 359–383.
- Wang, S., and F. Zhang (2010), Source of gravity waves within a vortex-dipole jet revealed by a linear model, *J. Atmos. Sci.*, *67*, 1438–1455.
- Wang, S., F. Zhang, and C. Snyder (2009), Generation and propagation of inertia-gravity waves from vortex dipoles and jets, *J. Atmos. Sci.*, *66*, 1294–1314.
- Williams, P. D., T. W. N. Haine, and P. L. Read (2008), Inertia-gravity waves emitted from balanced flow: Observations, properties, and consequences, *J. Atmos. Sci.*, *65*, 3543–3556.
- Yasuda, Y., K. Sato, and N. Sugimoto (2015a), A theoretical study on the spontaneous radiation of inertia-gravity waves using the renormalization group method. Part I: Derivation of the renormalization group equations, *J. Atmos. Sci.*, *72*, 957–983.
- Yasuda, Y., K. Sato, and N. Sugimoto (2015b), A theoretical study on the spontaneous radiation of inertia-gravity waves using the renormalization group method. Part II: Verification of the theoretical equations by numerical simulation, *J. Atmos. Sci.*, *72*, 984–1009.
- Zhang, F. (2004), Generation of mesoscale gravity waves in upper-tropospheric jet-front systems, *J. Atmos. Sci.*, *61*, 440–457.
- Zülicke, C., and D. H. W. Peters (2006), Simulation of inertia-gravity waves in a poleward breaking Rossby wave, *J. Atmos. Sci.*, *63*, 3253–3276.
- Zülicke, C., and D. H. W. Peters (2008), Parameterization of strong stratospheric inertia-gravity waves forced by poleward breaking Rossby waves, *Mon. Weather Rev.*, *136*, 98–119.